Stability in Composite Bearing Structures within Room-and-Pillar Goafs under Repeated Mining

Wenyu Lv[1], Lei Gao[1,*], Yongping Wu[1], Panshi Xie[1], Chao Lyu[1], Ru You[1], Tianqi Song[1] and Shijie Li[2]

[1] College of Energy and Mining Engineering, Xi'an University of Science and Technology, Xi'an, 710054, China

[2] Weinan Shaanxi Coal Qichen Technology Co., Ltd., Xi'an, 710054, China

INFORMATION

Keywords:
Repeated mining operations
backfill mining
room-and-pillar goaf
backfill body
failure stage

DOI: 10.23967/j.rimni.2025.10.67004

Revista Internacional de Métodos Numéricos para Cálculo y Diseño en Ingeniería

Stability in Composite Bearing Structures within Room-and-Pillar Goafs under Repeated Mining

Wenyu Lv[1], Lei Gao[1,*], Yongping Wu[1], Panshi Xie[1], Chao Lyu[1], Ru You[1], Tianqi Song[1] and Shijie Li[2]

[1]College of Energy and Mining Engineering, Xi'an University of Science and Technology, Xi'an, 710054, China

[2]Weinan Shaanxi Coal Qichen Technology Co., Ltd., Xi'an, 710054, China

ABSTRACT

During repeated mining of shallow and closely spaced coal seams, the failure of coal pillars within the upper goaf can induce dynamic hazards—such as shield jamming, support collapse, and roof fall—at the lower fully mechanized working face. To assess the stability of composite bearing structures, this study adopts a comprehensive approach that integrates orthogonal experimental design with single-factor experiments, supported by numerical simulation methods. Firstly, a composite bearing structure model is developed based on the engineering conditions of the Xingelao Coal Mine, followed by a comprehensive mechanical analysis. Secondly, experimental variables such as cement content, fly ash content, river sand content, and solid/slurry concentration are considered to systematically analyze their impact on backfill strength through proportion adjustment experiments. Furthermore, the controlled variable method is applied to adjust the backfill ratio, ultimately determining the optimal backfill mix ratio S8-2/3, which demonstrates a 7-day uniaxial compressive strength of 2.70 MPa with a backfill ratio of 2/3. This ratio satisfies both the mine's strength requirements and cost-effectiveness criteria. Based on this, a failure model for the "backfill-pillar" composite bearing structure is established by integrating stress-strain curves with observed failure modes during load-bearing processes. Finally, numerical simulation software was utilized to perform a stability analysis on both the composite load-bearing structure formed by post-backfilling in the room-and-pillar goaf and the overlying strata of the mined-out area. Numerical simulation results indicate that, under repeated mining conditions, the use of S8-2/3 backfilling material in room-and-pillar goafs significantly enhances the load-bearing capacity of residual coal pillars. It also effectively controls overburden movement and supports the safe and efficient extraction of coal resources.

OPEN ACCESS

Received: 23/04/2025

Accepted: 16/06/2025

Published: 22/09/2025

DOI
10.23967/j.rimni.2025.10.67004

Keywords:
Repeated mining operations
backfill mining
room-and-pillar goaf
backfill body
failure stage

*Correspondence: Lei Gao (gaolei0115@stu.xust.edu.cn).

1 Introduction

The room-and-pillar mining method was predominant during the early stages of China's reform and opening-up period. However, the strength of residual pillars gradually diminishes over time, and their potential failure can trigger a domino-type chain reaction, which may lead to significant surface subsidence [1–4]. Currently, the primary protective measure for remaining coal pillars in gob areas involves scattered grouting, in which grouting materials are used to reinforce the coal pillars. This reinforcement helps the pillars maintain their load-bearing capacity for the overlying strata under mining-induced disturbances from lower working faces, thereby preventing shield failure during subsequent mining operations [5,6]. Therefore, the primary challenge in ensuring the safe extraction of the lower coal seam lies in controlling the movement of overlying strata in room-and-pillar goaf areas through a composite support system consisting of filling bodies and coal pillars. This challenge can be further addressed by investigating the synergistic action mechanism of the filling body-coal pillar composite support system.

During longwall mining in the lower coal seams beneath a room-and-pillar goaf, the advancing abutment pressure leads to the redistribution of loads on the pillars. In extreme cases, this can result in pillar failure and overburden deformation [7–9], presenting significant challenges to extraction operations in the underlying coal seams. In studies on the mechanism of roof instability-induced disasters in room-and-pillar goaf areas, researchers have consistently highlighted the crucial role of pillar stability in preventing catastrophic failures. Lee et al. [10] and Hummel et al. [11] conducted a numerical simulation analysis to investigate the failure modes and failure locations of coal pillars in stope areas with room-and-pillar mining under the premise of fixed backfill material properties. Their study concluded that the width-to-height ratio of the coal pillar is a critical parameter in enhancing the stability of the room-and-pillar stope. Salmi et al. [12], through a study on the stability of coal pillars in abandoned room-and-pillar mining areas, employed numerical simulations to demonstrate that coal pillar aging plays a significant role in the long-term stability of shallowly buried abandoned room-and-pillar stope areas. Additionally, recommendations for enhancing the stability of coal pillars were proposed. Kim et al. [13] designed four stability enhancement strategies for coal pillars in room-and-pillar mining areas, including coal pillar overlap, coal pillar stiffness, coal pillar width, and the distance between coal pillars. The study concluded that coal pillar stiffness has the greatest impact on the stability of room-and-pillar stope areas. Abbasi [14] utilized the FLAC3D numerical simulation software to model the backfilling of stope areas and observed the impact of the backfill on the overlying strata and surface subsidence. The study concluded that backfilling effectively controls both the overlying strata and surface subsidence. Baryshnikov et al. [15] proposed the use of backfilling in room-and-pillar mining areas to enhance the stability of coal pillars, thereby preventing the collapse of overlying strata during the extraction of coal bodies at the bottom of open-pit mines. Franqueira and Paneiro [16], O'Sullivan [17], and Adach-Pawelus [18] filled room-and-pillar mining areas with different backfill materials and evaluated the overall and local stability of the stope areas post-filling using finite element analysis.

Although the aforementioned researchers have identified coal pillars as the key factor in stabilizing the roof of goaf areas and have recommended grouting to reinforce and protect these pillars, a critical scientific issue remains unresolved. Specifically, under repeated mining-induced disturbances, there is a lack of systematic investigation into the influence of filling material strength parameters and filling ratio on the stability of the "filling body-coal pillar" composite bearing structure. Based on previous studies, this work goes beyond simply filling room-and-pillar goaf areas with high-strength materials to enhance coal pillar bearing capacity. By optimizing the filling ratio according to actual mine conditions, it achieves both improved structural support and greater economic efficiency.

Therefore, this study proposes a backfill-pillar composite bearing structure model, grounded in the research framework of composite mechanical modeling, with a focus on the stability of coal pillars in shallow-buried room-and-pillar goaf systems and the requirements for overburden control. Through experimental investigation, the study examines the composite bearing structure formed by combining backfills with varying strengths and filling ratios with coal pillars, referred to as the backfill-coal pillar system. Through experimental investigation of the composite bearing structure formed by combining coal pillars with backfill materials of varying strengths and filling ratios, uniaxial compression tests were conducted to examine the strength enhancement mechanisms and failure progression stages of the backfill-coal pillar composite system. Furthermore, theoretical analysis is conducted to determine the minimum coal pillar bearing capacity required to ensure safe mining operations. Additionally, FLAC3D numerical simulation software was employed to conduct engineering-scale simulations based on the geological and mining conditions of the Xingelao Coal Mine, thereby validating the model's effectiveness in preserving coal pillar integrity and ensuring overburden stability. If the composite bearing structure can effectively maintain its structural integrity under repeated mining-induced disturbances, enhancing the stability of gob-side coal pillars will not only facilitate the control of overlying strata movement but also ensure the safety of mining operations in lower working faces, while simultaneously providing valuable technical insights for similar engineering scenarios.

2 Model Development and Analytical Study of Composite Bearing Structures

2.1 Experimental Context and Model Idealization

When the coal pillars in a room-and-pillar mined area are subjected to overburden stress caused by the mining of adjacent coal seams, stress concentration develops on the coal pillars, which accelerates their progression into the failure stage [19–21]. When the fully-mechanized mining face advances beneath a damaged coal pillar, the overlying rock strata collapse, triggering a chain reaction failure in the roof structure of the goaf area. During this process, the overlying strata above the fully mechanized working face undergo complete fracturing, preventing the formation of a stable load-bearing structure. Consequently, the support resistance of the hydraulic supports increases sharply, as illustrated in Fig. 1a. Grouting is performed in the room-and-pillar goaf area to establish a composite bearing structure through the synergistic interaction between the grout filling and the residual coal pillars. This engineered system allows the coal pillars to maintain their structural integrity and stability while providing adequate bearing capacity under roof instability conditions induced by mining disturbances from underlying fully-mechanized working faces. The proposed methodology effectively mitigates the risks of hydraulic support compaction and structural damage in the fully-mechanized mining face, as shown in Fig. 1b.

The backfill-coal pillar composite bearing structure essentially utilizes the confining pressure exerted by the backfill material to enhance the uniaxial compressive strength of the coal pillar. This transforms the original uniaxial loading condition of the coal pillar into a composite state-triaxial compression in the lower portion confined by the backfill and uniaxial compression in the upper portion. Such a configuration not only significantly improves the load-bearing capacity of the coal pillar but also limits its failure, while reducing overall backfilling costs. The engineering structural model of the backfill-coal pillar composite bearing structure is developed based on the following assumptions and simplifications: (1) The goaf floor maintains a uniform horizontal elevation without surface irregularities; (2) The remaining coal pillars in the goaf have regular geometric configurations with standardized dimensions; (3) The backfill material fully encapsulates the coal pillars, forming an integrated bearing structure; (4) The backfill slurry maintains a consistent mass concentration

throughout the vertical profiles, disregarding grout loss from the cement-fly ash mixture and material segregation in the analysis.

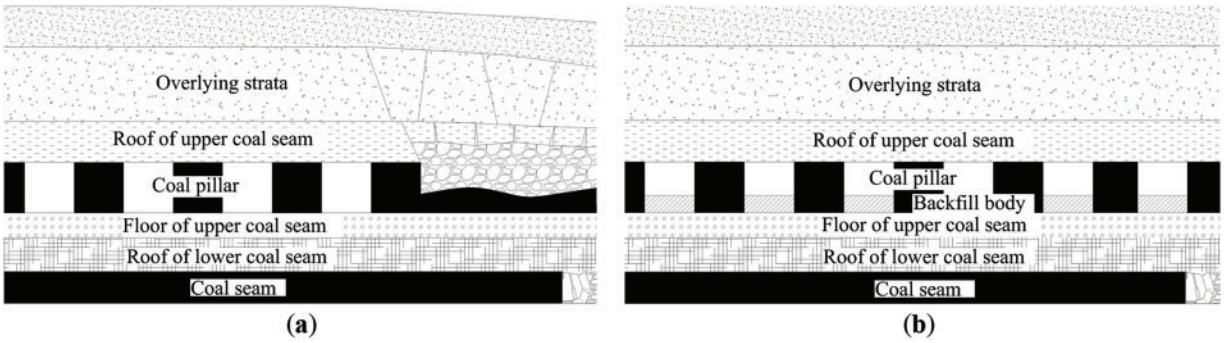

Figure 1: Engineering structure of the "filling body-coal pillar" composite load-bearing body (a,b). (a) Pillar failure in the goaf induced by the extraction of the lower coal seam; (b) "Filling body-coal pillar" composite bearing body supporting the overburden

Based on the aforementioned assumptions and analysis, the experimental methods of current backfill technologies for mined-out areas were referenced [22–25], a laboratory model and the corresponding simplified model of the backfill body-coal pillar composite load-bearing structure were developed, as illustrated in Fig. 2.

Figure 2: Composite load-bearing structure (a,b). (a) Composite load-bearing structure engineering model; (b) Cross-sectional view of composite load-bearing structure indoor experimental model

2.2 Stability Analysis of Coal Pillars and Roof Strata Beams in Goaf Areas

2.2.1 Analysis of Load-Bearing Characteristics of Coal Pillars in Room-and-Pillar Mined-Out Areas

Upon completion of room-and-pillar mining operations, uniformly distributed cubic coal pillars of equal dimensions are left between the extracted rooms, within the same area and operational period. At the mined-out room locations, the roof strata lose their support, causing the overburden stress to be fully transferred to the coal pillars. Due to the high similarity in geometric and mechanical properties, coal pillars can be treated as uniformly distributed bearing elements supporting the roof load. Given the high similarity among coal pillars, it can be assumed that the roof load is uniformly shared by the pillars. Accordingly, the vertical stress borne by each coal pillar comprises not only the overburden stress directly above the pillar itself, but also half of the overburden stress from the adjacent coal

rooms. Fig. 3 presents a schematic diagram illustrating the distribution and stress state of coal pillars within the goaf area.

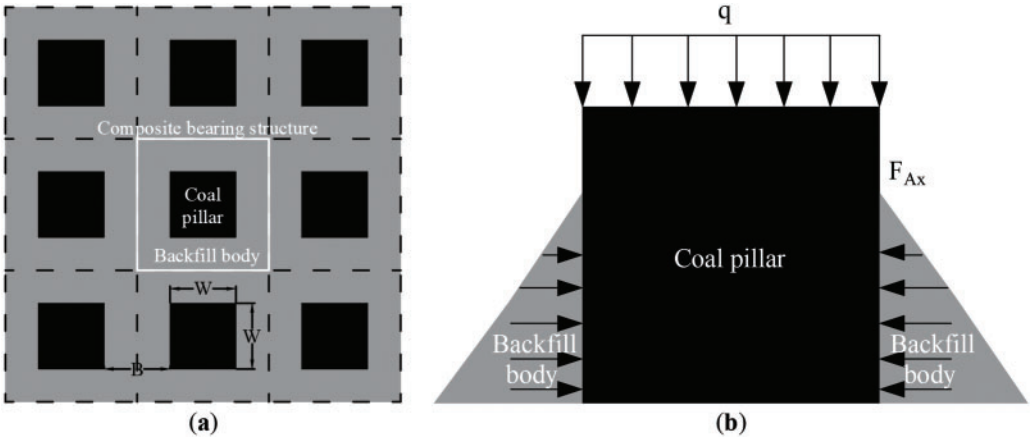

Figure 3: Composite load-bearing structure (a,b). (a) Composite load-bearing structure engineering model; (b) Cross-sectional view of composite load-bearing structure indoor experimental model

In calculating the bearing stress of coal pillars, the room width must be considered, as shown in Eq. (1):

$$q = \frac{\gamma h(W + B)^2}{W^2} \tag{1}$$

In this formula, q represents the uniformly distributed load borne by the coal pillar in the vertical direction (MPa); γ denotes the average unit weight of the overlying strata in the room-and-pillar goaf (kN/m^3); h indicates the burial depth of the No. 5^{-2} coal seam (m); W stands for the width of the coal pillar in the goaf (m); and B refers to the width of the extracted mining room (m).

The parameter values for various sections in the experimental mine are listed in Table 1.

Table 1: Experimental mine coal seam parameter table

Unit weight of overlying strata $\boldsymbol{\gamma}$/KN/m^3	Burial depth of coal seam h/m	Coal pillar width W/m	Coal room span B/m
23	84	5	5

By substituting the parameters from Table 1 into Eq. (1) for computational analysis, the uniformly distributed load borne by the coal pillar was calculated to be 7.73 kN/m^2.

2.2.2 Mechanical Analysis of Roof Stratum Beam

Under partial backfill conditions, unreinforced coal pillars in room-and-pillar goaf areas can be classified into failure and non-failure states based on specific backfill parameters. Therefore, when analyzing the roof rock beam in room-and-pillar goaf areas under partial backfill conditions, distinct mechanical models of the roof can be established according to the two different mechanical states of the coal pillars.

Fig. 4 presents the mechanical analysis model of the roof rock beam under the condition of an intact coal pillar providing stability. In this model, the uniformly distributed load q_1 applied to the upper surface of the rock beam represents the resultant force, which is composed of the vertical stress induced by the overlying strata and the abutment pressure from the working face at the forefront. Since both components can be considered uniformly distributed loads with consistent directions, they are mathematically combined into a simplified equivalent load q_1 for analytical convenience. It is known that the room-and-pillar goafs above the 53,201 working face of the Xingelao Coal Mine are uniformly distributed and were formed simultaneously through drill-and-blast mining. Therefore, the bearing capacities provided by the coal pillars to the roof can be considered similar. According to Eq. (1), the load-bearing capacity of each coal pillar can be approximated as one-fourth of the uniformly distributed roof load. For simplification in subsequent calculations, the coal pillar bearing capacity is denoted as $4q_2$. The rock beam in the unexcavated section of the working face retains its structural integrity and can be idealized as having fixed boundary conditions at both ends.

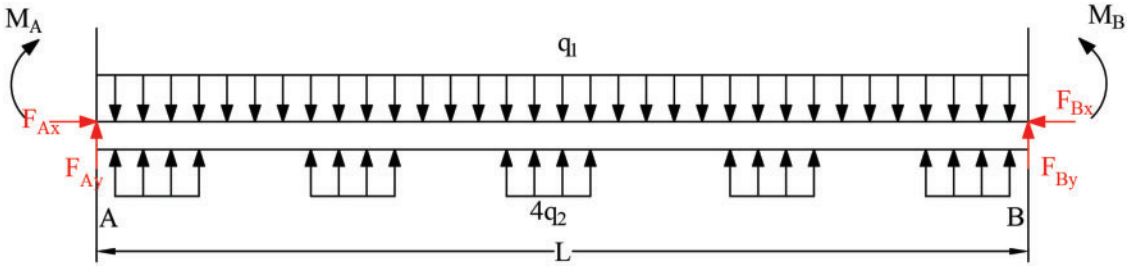

Figure 4: Mechanical model of roof with intact coal pillars

Fig. 5 illustrates the equivalent mechanical analysis model of the roof rock beam under intact coal pillar conditions. According to the principle of equivalent force in solid mechanics, when both the roof strata and coal pillar retain their structural integrity, the segmented bearing load exerted by the coal pillar can be treated as a uniformly distributed load. As shown in Eq. (1), when the bearing capacity of coal pillars is equivalently converted into a uniformly distributed load on the roof, the magnitude of this equivalent load is one-fourth of the coal pillar's bearing capacity, denoted as q_2. A Cartesian coordinate system is established with point A, located at the left end of the rock beam, as the origin. The X-axis aligns with the strike direction of the working face, and the Y-axis is oriented perpendicular to the roof strata.

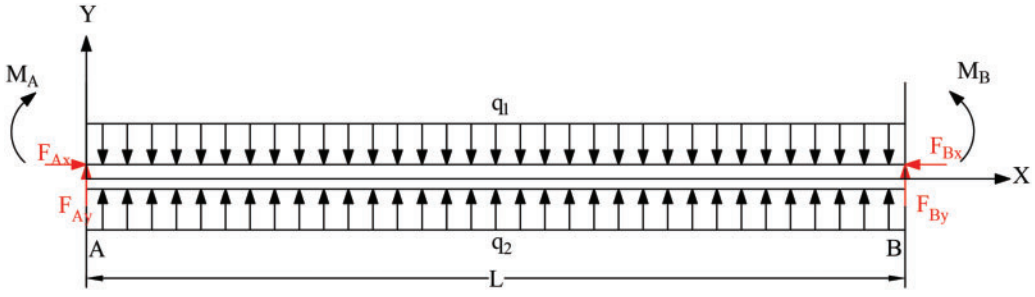

Figure 5: Equivalent mechanical model of roof supported by intact coal pillars

Based on the principles of theoretical mechanics, the reaction forces at both ends of the rock beam can be mathematically represented as follows:

$$F_{Ax} = F_{Bx} = 0 \tag{2}$$

$$F_{Ay} = F_{By} = \frac{(q_1 - q_2)}{2} L \tag{3}$$

According to the principles of engineering mechanics, the governing differential equation for the deflection of the rock beam segment AB can be expressed as follows:

$$y''(x) = \frac{(q_1 - q_2) L}{2EI} x - \frac{(q_1 - q_2)}{2EI} x^2 \tag{4}$$

The subjects of Eqs. (3) and (4) are treated under the assumption that the rock beam behaves as a unified structure. Nevertheless, when analyzing a single coal pillar, a distinct approach is necessary. These conditions are valid solely for determining the maximum displacement and maximum load at the center of the rock beam.

Based on the principles of engineering mechanics and material mechanics, the deflection and rotational angle equations for the rock beam can be derived as follows:

$$y(x) = -\frac{1}{EI}\left[\frac{(q_1 - q_2) L}{2} \times \frac{x^3}{6} - \frac{(q_1 - q_2)}{2} \times \frac{x^4}{12}\right] \tag{5}$$

$$\theta(x) = -\frac{1}{EI}\left[\frac{(q_1 - q_2) L}{2} \times \frac{x^2}{2} - \frac{(q_1 - q_2)}{2} \times \frac{x^3}{3}\right] \tag{6}$$

In the equation, E and I denote the elastic modulus and moment of inertia of the roof rock beam, respectively, as determined through field measurements, while L represents the length of the working face.

The bending moment equation for the roof rock beam is:

$$M(x) = \frac{(q_1 - q_2) L}{2} x - \frac{(q_1 - q_2)}{2} x^2 \tag{7}$$

Based on the preceding analysis and considering that the bending moment equation is a quadratic function, the maximum bending moment is expected to occur at the midspan (L/2) of the structural model. The expressions for the bending moment, deflection, and rotation at this critical point can therefore be derived as shown in Table 2:

Table 2: Critical point analysis of roof strata beam in underground mining structures

Peak bending moment point	Bending moment	Deflection	Rotation angle
L/2	$\frac{(q_1 - q_2) L^2}{8}$	$-\frac{(q_1 - q_2) L^4}{32EI}$	$-\frac{(q_1 - q_2) L^3}{16EI}$

Based on the data presented in Table 2, it can be inferred that when the roof rock beam is subjected to bending forces, the maximum deformation occurs at the midspan (L/2). This indicates that the coal pillars at the midspan position (L/2) bear the maximum roof load, while the load exerted by the roof on

the coal pillars decreases gradually toward both ends. Therefore, when failure occurs in a coal pillar, it originates from the central section of the working face, triggering a "domino effect" on adjacent coal pillars. The failure then propagates toward both ends until roof caving takes place, resulting in stress relief.

As illustrated in Fig. 6, when constructing the mechanical model, it is assumed that the fractured roof strata in the central region have experienced tensile failure due to the collapse of the coal pillar. Therefore, the rock beam can be modeled as a cantilever beam. The sections adjacent to both ends of the coal pillar remain intact, continuing to provide effective support to the overlying roof strata and maintaining their load-bearing capacity.

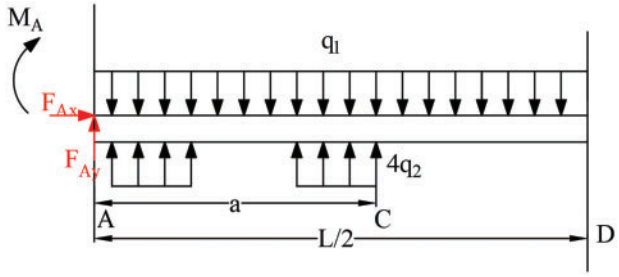

Figure 6: Mechanical model of roof under coal pillar failure

Consistent with the equivalent mechanical model of the roof beam under intact coal pillar conditions, an equivalent stress analysis is conducted for the roof mechanical model considering coal pillar failure. As illustrated in Fig. 7, a Cartesian coordinate system is established within the mechanical model, and the stress distribution of the roof beam is analyzed accordingly.

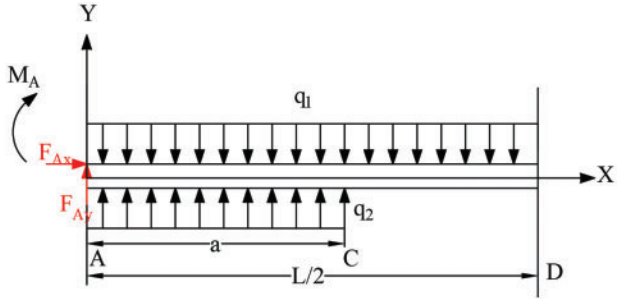

Figure 7: Equivalent mechanical model of roof under coal pillar failure

$$F_{Ax} = 0 \tag{8}$$

$$F_{Ay} = \frac{q_1 L}{2} - q_2 a \tag{9}$$

$$M_A = 0 \tag{10}$$

For analytical convenience, the rock beam is divided into two segments (AC and CD) for separate mechanical analysis. The differential equations governing the deflection of segments AC and CD are derived as follows:

$$y''_{AC}(x) = \frac{(q_1 - q_2)}{2EI} x^2 \tag{11}$$

$$y''_{CD}(x) = \frac{q_1}{2EI}x^2 - \frac{q_2 a}{EI}\frac{(x-a)}{2} \tag{12}$$

Based on the principles of engineering mechanics and material mechanics, the deflection and rotational angle equations for the rock beam can be derived as follows:

$$y_{AC}(x) = \frac{1}{EI}\left(\frac{q_1 x^4}{24} - \frac{q_2 x^4}{24}\right) \tag{13}$$

$$y_{CD}(x) = \frac{1}{EI}\left(\frac{q_1 x^4}{24} - \frac{q_2 a x^3}{12} + \frac{q_2 a x^2}{4} + \frac{q_2 a^3 x}{12} - \frac{q_2 a^2 x}{2}\right) + \frac{q_2 a^3}{4EI} - \frac{q_2 a^4}{24EI} \tag{14}$$

$$\theta_{AC}(x) = \frac{1}{EI}\left(\frac{q_1 x^3}{6} - \frac{q_2 x^3}{6}\right) \tag{15}$$

$$\theta_{CD}(x) = -\frac{1}{EI}\left(\frac{q_1 x^3}{6} - \frac{q_2 a^2 x^2}{4} + \frac{q_2 a x}{2}\right) + \frac{q_2 a^3}{12EI} - \frac{q_2 a^3}{2EI} \tag{16}$$

In the formula, EI represents the flexural rigidity of the roof strata, a denotes the strike-directional length of the intact zone in the coal pillar (unaffected by failure), and L indicates the length of the working face along the panel strike.

The bending moment equation for the roof rock beam is:

$$M_{AC}(x) = \frac{(q_1 - q_2)}{2}x^2 \tag{17}$$

$$M_{CD}(x) = \frac{q_1}{2}x^2 - \frac{q_2 a\,(x-a)}{2} \tag{18}$$

Based on the comprehensive analysis above, the expressions for the bending moment, deflection, and rotation angle at the critical failure point of the coal pillar are derived and summarized in Table 3.

Table 3: Critical point analysis table for coal pillar failure

Critical threshold parameter	Bending moment	Deflection	Rotation angle
a	$\frac{(q_1 - q_2)\,a^2}{2}$	$\frac{1}{EI}\left(\frac{q_1 a^4}{24} - \frac{q_2 x^4}{24}\right)$	$\frac{1}{EI}\left(\frac{q_1 a^3}{6} - \frac{q_2 a^3}{6}\right)$

Based on the aforementioned analysis, it is reasonable to infer that stress concentration will occur in the central region of the working face under partial backfilling conditions. In this critical zone, both deflection and rotation angles reach their maximum values earlier than in other areas, indicating a higher likelihood of failure in the roof strata and coal pillars. Such failures could pose potential risks to mine production. In contrast, coal pillars located closer to the lateral boundaries experience progressively lower levels of stress concentration, thereby reducing the risk of structural instability. Subsequent investigations should prioritize a comprehensive analysis of the mechanical behavior exhibited by composite bearing structures under stress concentration conditions at the mid-section working face. This research direction is crucial for ensuring the structural stability and load-bearing efficacy of roof support systems in room-and-pillar goaf areas during the No. 5^{-3} coal seam extraction operations.

3 Mechanical Property Testing of Backfill and Composite Load-Bearing Medium

3.1 Orthogonal Experimental Design of Mix Proportions for Backfill Mechanical Properties

The materials used for the experimental backfill were based on the filling compositions investigated in the studies of other researchers [26–29]. These compositions included coal gangue with a specified gradation, river sand, cement, and fly ash. In this material system, cement served as the primary cementitious binder, while gangue and river sand acted as coarse and fine aggregates, respectively. Fly ash was incorporated as a partial replacement for cement to enhance the performance of the cementitious matrix. To maximize the utilization of the inherent mechanical properties of the gangue, an optimal gradation parameter of $n = 5$ was selected based on the mining conditions of Xingelao Coal Mine. The gangue particle size distribution was as follows: particles sized 0–5 mm accounted for 58%, those in the 5–10 mm range constituted 27%, and particles sized 10–15 mm represented 15% of the total mass. To investigate the influence of cement content, fly ash dosage, river sand content, and slurry concentration on the mechanical behavior of the backfill-coal pillar composite bearing structure, an orthogonal experimental design was developed with four variables: cement content (A) at 4%, 6%, and 8%; fly ash dosage (B) at 13%, 14%, and 15%; slurry concentration (C) at 78%, 80%, and 82%; and river sand content (D) at 16%, 24%, and 32%. Cubic molds with dimensions of 50 mm and 100 mm were used to prepare the test specimens. After demolding, specimens with smooth surfaces and minimal air bubbles were selected. These specimens were cured to different ages: 7, 14, 21, and 28 days. Uniaxial compressive strength (UCS) tests were conducted at each curing age. The loading rate was set at 10 mm/s. A total of 9 groups of tests were designed, with 3 specimens tested per group. In total, 108 qualified specimens were prepared and tested. All data were recorded and analyzed. Table 4 presents the grouping of the tests and the average UCS at each curing age.

Table 4: Orthogonal experimental levels for the backfill material

Number	A/%	B/%	C/%	D/%	Average UCS/MPa			
					7 d	14 d	21 d	28 d
S1	4	13	78	16	1.65	3.84	4.81	5.40
S2	4	14	80	24	2.06	4.14	5.02	5.71
S3	4	15	82	32	2.38	4.79	5.33	6.18
S4	6	13	82	24	2.26	4.50	5.39	6.03
S5	6	14	78	32	2.13	4.68	5.40	6.46
S6	6	15	80	16	2.10	4.35	5.16	6.06
S7	8	13	80	32	2.55	5.10	5.88	6.77
S8	8	14	82	16	2.70	5.06	5.68	6.52
S9	8	15	78	24	2.26	5.02	5.73	6.65

As shown in Fig. 8, the 7 d UCS initially increases and then decreases with the increase in fly ash dosage (B), while it consistently increases with the rise in parameters A, C, and D. Regarding the UCS of cemented paste backfill, the order of significance of the influencing factors is A > C > D > B, with cement content being the primary factor affecting backfill strength. Consequently, the optimal combination for maximizing backfill strength is S8, corresponding to a cement content of 8%, a slurry concentration of 82%, a river sand content of 16%, and a fly ash content of 14%. The 14, 21, and 28 d uniaxial compressive strengths increase to varying extents with the rise in parameters A, B, C, and D.

The order of significance of the influencing factors is A > D > B > C, with cement content identified as the primary factor affecting the strength of the cemented paste backfill. Consequently, the optimal combination for maximizing backfill strength is S7, which corresponds to a cement content of 8%, a river sand content of 32%, a slurry concentration of 80%, and a fly ash content of 13%.

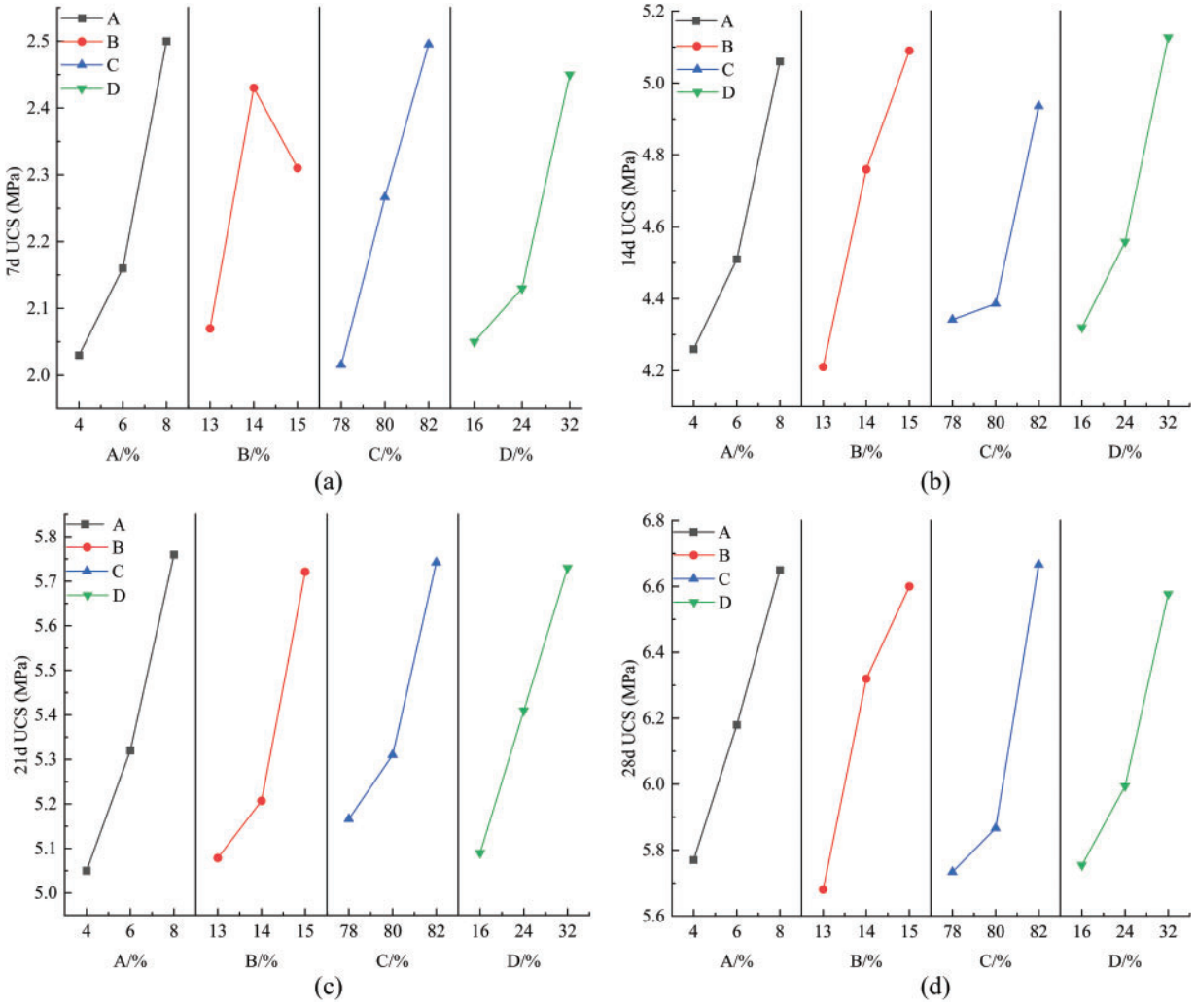

Figure 8: Relationship between UCS and multiple factors (a–d). (a) Relationship between 7-day UCS and multiple factors; (b) Relationship between 14-day UCS and multiple factors; (c) Relationship between 21-day UCS and multiple factors; (d) Relationship between 28-day UCS and multiple factors

In summary, the influencing factors exhibit slightly different effects on the early and later strength development of the backfill material. Considering the impact of 5^{-3} seam mining in the Xingelao Coal Mine on the bearing capacity of coal pillars in the overlying room-and-pillar goaf, as well as the long-term support function of these pillars for the overburden, a comprehensive conclusion can be drawn. The backfill material must provide sufficient strength not only in the early stage to ensure safe extraction of the 5^{-3} seam, but also in the later stage to effectively sustain the roof of the room-and-pillar goaf. Therefore, it is recommended to select the backfill materials with mix ratios S7 and S8 for subsequent experiments. If the 7 d UCS of the S7 and S8 backfills can provide stable support

for the roof strata of the pillar-type goaf, then backfill strengths exceeding 2.55 or 2.70 MPa will also be effective in ensuring stable support for the goaf roof.

3.2 Strength Testing of Composite Bearing Structures with Varied Backfill Ratios

Based on previous research [16,22,26], in the backfill-coal pillar composite bearing structure, the lower backfill body remains intact until the failure of the upper unfilled coal pillar section. This mechanism allows the backfill material to continuously provide stable confining pressure to the reinforced coal pillar, thereby maintaining the lower backfilled coal pillar in a triaxial stress state that enhances its bearing capacity. Based on this mechanical characteristic, this study proposes using uniaxial compression testing to determine the strength parameters of the composite bearing structure.

The backfill ratio is a key factor influencing the stability of coal pillars following backfilling operations. In mining engineering applications, an appropriate backfill ratio not only prevents structural failure of coal pillars under specific geological conditions, but also significantly affects their failure mechanisms and temporal evolution. Additionally, the backfill ratio plays a vital role in the redistribution of stress within the surrounding rock mass. This is especially critical during the extraction of adjacent seams in room-and-pillar goafs. Under such conditions, optimizing the backfill ratio is essential, as it directly impacts the control of stress transfer and the long-term structural stability of the mining system.

To investigate the influence of backfill ratios on the mechanical properties of the backfill body-coal pillar composite bearing structure, the backfill ratios were designed as 0, 1/5, 1/3, 1/2, 2/3, 3/4, and 1. To effectively backfill the upper room-and-pillar goaf and ensure roof stability in the lower fully mechanized working face, it is essential to select an appropriate backfill strength. In addition, production efficiency and actual operational conditions of the experimental mine must be considered. Therefore, the 7 d UCS of the backfill material was adopted as the reference criterion for determining the backfill strength in subsequent experimental procedures. Based on the analysis in the previous section, both mix proportions S7 and S8 were selected for the backfill materials, with corresponding 7 d UCS values of 2.55 and 2.70 MPa, respectively. The prepared slurry was thoroughly mixed and poured into 100 mm × 100 mm × 100 mm cubic molds. Different filling ratios (0, 1/5, 1/3, 1/2, 2/3, 3/4, 1) were achieved by varying the casting height around the central coal pillar cube within the mold. After demolding and curing for 7 days, the composite bearing specimens were subjected to uniaxial compression tests at a loading rate of 0.05 MPa/s. The strength enhancement effects of coal pillars under different filling ratios were systematically recorded through this experimental procedure. Table 5 presents the UCS values and strength enhancement effects of composite bearing structures with backfill material mix ratios S7 and S8 under different filling proportions.

As shown in Table 5 and Fig. 9, both S7 and S8 specimens demonstrated a progressive increase in UCS and the strength enhancement effect of the composite backfill with rising filling ratios. Notably, the 1/2 filling ratio appeared to be a critical threshold in this strengthening mechanism. When the backfill mix ratio is S7 and the filling proportion is less than 1/2, the composite bearing structure shows a notable enhancement in strength. The strength improvement increases from 100% to 140.96%. This corresponds to a net gain of 40.96% in load-bearing capacity. However, when the filling proportion exceeds 1/2, the strength improvement of the composite bearing structure progresses at a slower rate, increasing from 140.96% to 165.90%, with a marginal gain of 24.94%. When the backfill mix ratio is S8 and the filling proportion is less than 1/2, the composite bearing medium exhibits a pronounced strength enhancement, with the strength improvement increasing from 100% to 149.27%, representing a 49.27% increase. However, when the filling proportion exceeds 1/2, the strength improvement of

the composite bearing medium progresses more gradually, increasing from 149.27% to 178.39%, representing an incremental gain of 29.12%.

Table 5: Strength table of composite bearing bodies with different filling ratios

Number	Backfill strength/ MPa	Backfill ratio	Strength of composite bearing medium/MPa			Mean strength of composite bearing system/MPa	Strength enhancement of composite bearing structure/%
			Specimen a	Specimen b	Specimen c		
S7	2.55	0	–	–	–	4.81	100
S7-1/5	2.55	1/5	5.83	5.79	5.81	5.81	120.79
S7-1/3	2.55	1/3	5.91	5.90	5.92	5.91	122.87
S7-1/2	2.55	1/2	6.69	6.83	6.82	6.78	140.96
S7-2/3	2.55	2/3	7.61	7.32	7.54	7.49	155.72
S7-3/4	2.55	3/4	7.56	7.59	7.62	7.59	157.80
S7-1	2.55	1	7.81	8.09	8.04	7.98	165.90
S8	2.70	0	–	–	–	4.81	100
S8-1/5	2.70	1/5	5.96	6.04	5.97	5.99	124.53
S8-1/3	2.70	1/3	6.18	6.15	6.21	6.18	128.48
S8-1/2	2.70	1/2	7.21	7.19	7.14	7.18	149.27
S8-2/3	2.70	2/3	7.96	7.98	7.79	7.91	164.45
S8-3/4	2.70	3/4	8.19	8.23	8.34	8.22	170.89
S8-1	2.70	1	8.59	8.63	8.52	8.58	178.39

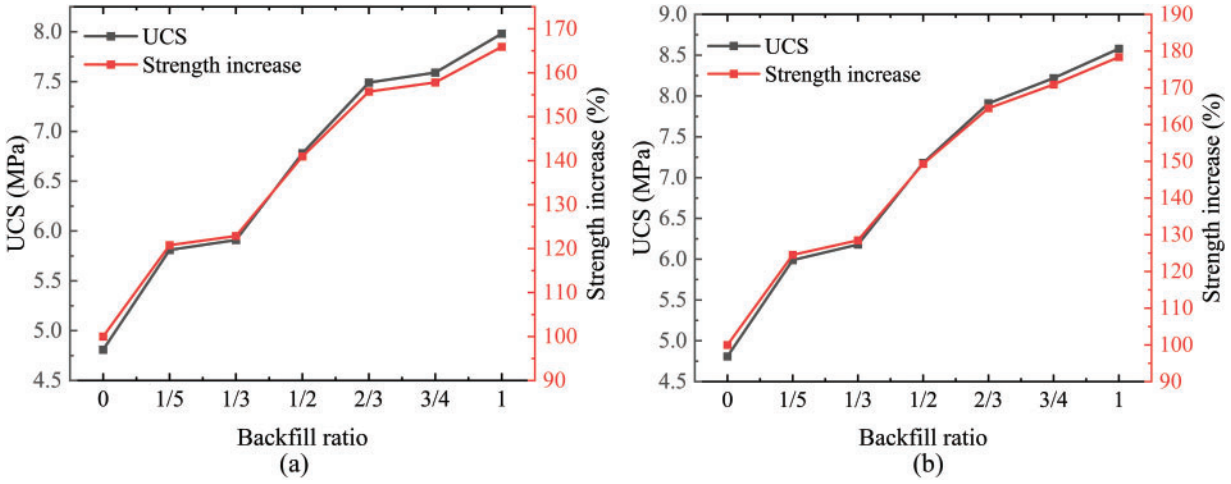

Figure 9: Influence of grout proportion on UCS at varying 7-day strength levels (a,b). (a) Influence of S7 grout proportion on compressive strength of backfill materials; (b) Influence of S8 grout proportion on compressive strength of backfill materials

Based on the mechanical analysis presented in Section 2, the average load borne by coal pillars in the 5^{-2} room-and-pillar goaf was determined to be 7.73 MPa. To ensure the safe and efficient extraction of the 5^{-3} coal seam while optimizing economic benefits, a filling plan of at least S8-2/3 should be adopted. This plan specifies a uniaxial compressive strength of 2.70 MPa after 7 days, a filling ratio of 2/3, and a composite bearing body strength of 7.91 MPa, which surpasses the required 7.73 MPa, thereby providing effective support for the overlying strata.

3.3 Analysis of Failure Characteristics in Composite Bearing Structures

Based on the analysis in Section 3.2, the composite bearing body with a filling ratio of 2/3 is selected as the research object. The failure process of this structure is analyzed in detail. Fig. 10 presents the uniaxial compression displacement-stress curve of the composite bearing body with a backfill ratio of 2/3. Based on the curve characteristics and failure pattern analysis, the failure mechanism can be divided into eight distinct phases: Compaction stage, linear elastic stage, plastic stage, upper section failure stage, loose mass sliding stage, compaction stage of loose bodies, complete failure stage of the coal pillar, and failure stage of the backfill.

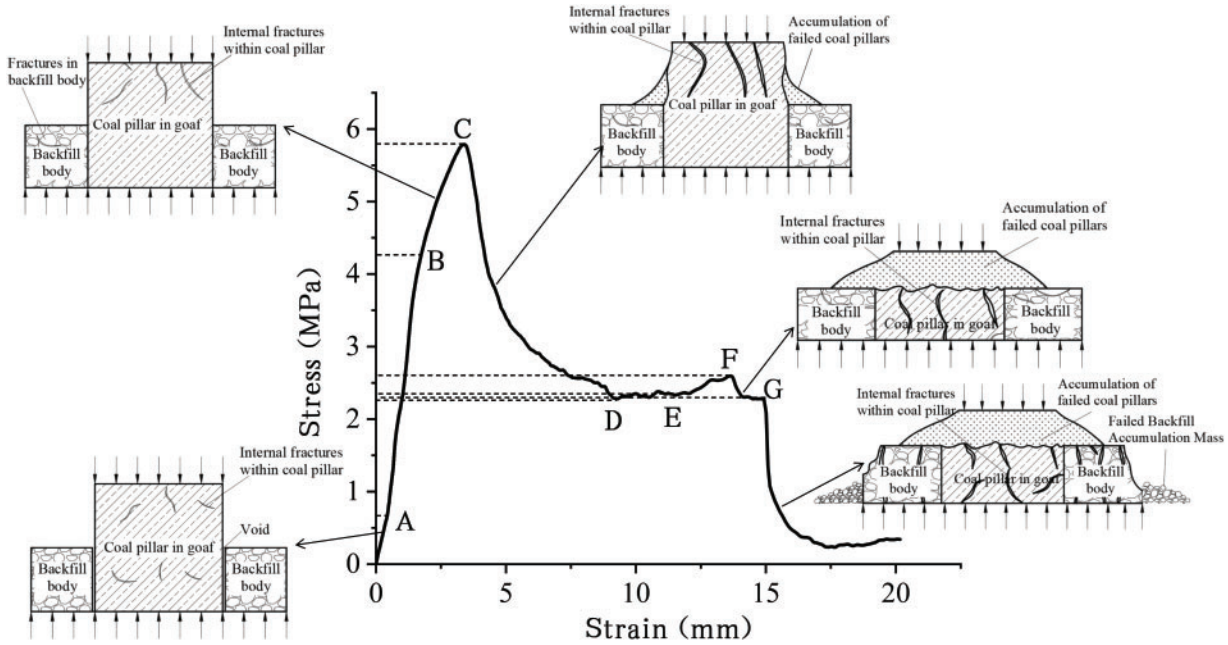

Figure 10: Uniaxial compression stress-displacement curve for composite bearing bodies. The coordinates of the inflection points in the figures are specifically identified as follows: A (0.43, 0.66); B (1.74, 4.27); C (3.44, 5.78); D (9.22, 2.28); E (12.03, 2.35); F (13.65, 2.59) and G (14.93, 2.27)

The damage mechanisms of the composite bearing structure during the loading process can be analyzed in eight distinct stages, as outlined below:

Compaction stage (0∼A): A microscopic gap exists between the backfill and the coal pillar, with the load being entirely supported by the central coal pillar. The deformation characteristics of the coal pillar are similar to those observed under unfilled conditions. Internal microfractures gradually close during loading. Meanwhile, lateral displacement remains minimal throughout the process. The self-deformation of the coal pillar does not result in significant stress transfer to the surrounding backfill material. The curve exhibits a concave-upward shape, indicating a progressive deceleration in the rate of stress intensification as deformation accumulates.

Linear elastic stage (A∼B): As the applied load increases, the internal microfractures within the backfilled coal pillar gradually close completely. Under longitudinal compressive loading, new microcracks initiate within the backfill specimen. Concurrently, the transverse strain of the coal pillar begins to progressively increase, gradually filling the micro-interstices between the coal pillar and the backfill material. This interaction results in mutual compression within the lower segment of the

composite bearing structure, where the backfill material exerts confining pressure on the underlying coal pillar. Notably, the primary development zone of microfractures is predominantly concentrated in the upper section of the coal pillar. The curve displays a linear progression, with stress and deformation showing a strong linear correlation.

Plastic stage (B∼C): Under compressive loading, microscopic fissures within the unfilled coal pillar gradually propagate and interconnect, ultimately merging into macroscopic fractures that lead to structural failure, resulting in a complete loss of load-bearing capacity. The backfill-reinforced coal pillar undergoes triaxial stress confinement, which effectively suppresses the development of internal fractures and enhances the yield strength of its load-bearing capacity. The backfill-reinforced coal pillar is subjected to triaxial compressive stresses, which effectively inhibit the development of internal fractures and enhance the material's yield strength limit. As a result, the backfill structure retains its integrity without exhibiting failure behavior. The curve primarily characterizes the failure mode of the upper coal pillar, showing a progressive deceleration in the rate of stress increase as deformation increases.

Upper section failure stage (C∼D): In the upper section of the coal pillar, macrocracks continue to propagate and interconnect, forming surface fractures and failure planes. The coal pillar undergoes crushing under compression, with fragmented material accumulating in the central region of the specimen. Meanwhile, the lower section experiences increased lateral displacement and more pronounced mutual extrusion with the backfill material, while still retaining some residual load-bearing capacity. The stress-deformation curve exhibits a pronounced stress drop with increasing deformation.

Loose mass sliding phase (D∼E): In this stage, the large block located in the upper section of the coal pillar undergoes sliding failure. This sliding failure results in a reduction in the height of the pillar, thereby decreasing the pressure exerted on the coal pillar. Although the longitudinal load decreases, the fractures formed in the lower section of the coal pillar do not fully recover to their original state, leading to a significant reduction in its load-bearing capacity. In this phase, the stress-deformation curve shows small amplitude oscillations within a defined range as deformation increases, indicating a quasi-stable yet weakened load-bearing state.

Compaction stage of loose bodies (E∼F): After the collapse of the upper loose blocks, the continued descent of the uniaxial hydraulic press results in an increase in the longitudinal stress exerted on the coal pillar. The inter-block voids undergo further compaction, with some blocks being crushed into powder to fill the gaps. Consequently, the applied pressure is directly transferred to the lower section of the coal pillar. The stress-deformation curve displays an upward concave profile, with stress gradually increasing to peak strength as deformation grows.

Complete failure stage of coal pillar (F∼G): Under continuous loading from the uniaxial hydraulic press, the pressure is transmitted directly through the compacted, fragmented blocks to the underlying composite bearing structure. This leads to further propagation of cracks within the lower composite bearing structure. As the ultimate strength has not yet been reached, the composite bearing structure does not experience significant fragmentation. The stress-deformation curve exhibits a characteristic decline to a stabilized value, with stress gradually decreasing as deformation increases.

Failure stage of backfill (G): At this stage, both the coal pillar and the backfill completely lose their load-bearing capacity. Although the external morphology of the backfill appears intact at point G, further loading initiates the propagation of internal macro-fractures. These fractures extend to the specimen surface and develop into through-going cracks across the composite structure. Subsequently, the outer backfill fractures and disintegrates, exposing the fully failed coal pillar. This phase is

characterized by a sharp decline in the stress-deformation curve, with stress rapidly decreasing as deformation increases.

In conclusion, the backfill material can significantly enhance the uniaxial compressive strength of coal pillars. However, prior to the failure of the upper coal pillar, fractures develop within the backfill, leading to a relatively limited strength improvement during the later stages of compression. This is evidenced by the significantly lower peak at point F compared to point C in the stress-strain curve. Therefore, it can be concluded that the composite bearing structure exhibits reduced load-bearing performance after the failure of the upper coal pillar, with a substantial decrease in bearing capacity.

4 Study on Stability Control of Overlying Strata and Coal Pillars in Goaf Areas

Partial grouting backfill of room-and-pillar goafs can effectively protect coal pillars. It enhances their load-bearing capacity. This approach helps prevent roof damage caused by mining-induced disturbances during lower seam extraction. As a result, it maintains the structural stability of coal pillars in room-and-pillar goafs. Building on the analysis in the previous chapter, FLAC3D numerical simulations were further employed to validate the deformation characteristics and damage extent of both the goaf roof and coal pillars under different backfill ratios. This study systematically investigates the impact of different backfill conditions on stress redistribution within room-and-pillar goaf systems and the associated migration patterns of the overburden strata. Particular emphasis was placed on quantifying the stress evolution mechanisms in coal pillars and analyzing the displacement patterns within the overlying rock formations under various backfill scenarios.

4.1 Numerical Modeling and Experimental Design

(1) Computing software

FLAC3D is a three-dimensional finite difference software developed by ITASCA Consulting Group, USA. Owing to its powerful computational capacity and versatile modeling capabilities, it has been widely applied in the coal mining industry. FLAC3D allows for intuitive visualization of simulation results, such as stress distribution, displacement fields, and plastic zones, typically presented as contour plots. These features make it a valuable tool for monitoring and evaluating the impacts of coal seam extraction. Due to its high computational efficiency, FLAC3D enables the simulation of complex mining scenarios through appropriate parameter input, boundary condition setting, and mesh discretization, thereby reducing time costs. Its simulation accuracy has been extensively validated and is widely recognized.

(2) Calculation parameters

The experiment was conducted using geological data from the 53,201 working face of the Xingelao Coal Mine. The specific mechanical parameters of the coal and rock are listed in Table 6.

In the numerical simulation, the Mohr-Coulomb criterion was adopted as the failure criterion to evaluate the damage state of the rock mass.

$$f_s = \sigma_1 - \sigma_3 \frac{1+\sin\varphi}{1-\sin\varphi} - 2c\sqrt{\frac{1+\sin\varphi}{1-\sin\varphi}} \tag{19}$$

In the formula, σ_1 and σ_3 are the maximum and minimum principal stresses, respectively; c and φ are the bonding force and the friction angle, respectively.

Table 6: Numerical simulation formation information table

Lithology	Elastic modulus (kg/m^3)	Density (MPa)	Poisson's ratio	Cohesion (MPa)	Thickness (m)	Internal friction angle (°)
Loess	1436	8.56×10^3	0.35	0.02	4.36	15
Siltstone	2432	16.36×10^3	0.29	0.32	5.30	32
Fine-grained sandstone	2360	24.52×10^3	0.28	0.72	5.51	32
Siltstone	2250	8.56×10^3	0.22	0.35	9.25	23
Fine-grained sandstone	2510	25.82×10^3	0.33	0.82	6.56	27
Medium-grained sandstone	2632	24.62×10^3	0.28	0.46	5.54	26
Siltstone	2165	7.56×10^3	0.25	0.36	8.22	32
Sandy mudstone	2398	13.52×10^3	0.26	0.08	8.68	22
Medium-grained sandstone	2550	21.56×10^3	0.32	0.51	9.42	26
Sandy mudstone	2523	14.73×10^3	0.25	0.08	3.95	21
Fine-grained sandstone	2520	24.42×10^3	0.32	0.69	5.30	33
Siltstone	2258	7.21×10^3	0.19	0.35	3.35	23
5^{-2} Coal seam	1382	2.65×10^3	0.18	0.63	3.55	21
Medium-grained sandstone	2670	23.02×10^3	0.29	0.43	9.92	27
Fine-grained sandstone	2394	27.55×10^3	0.31	0.72	2.15	31
5^{-3} Coal seam	1412	2.35×10^3	0.18	0.63	1.15	21
Siltstone	2330	18.57×10^3	0.24	0.39	4.26	26
Fine-grained sandstone	2570	25.65×10^3	0.32	0.81	2.32	31

When condition f_s is met, the material will undergo shear failure. It is a widely observed pattern that compressive strength ranks highest among the various mechanical properties, while tensile strength is typically the lowest. Therefore, the tensile failure of the rock mass is scientifically determined based on the tensile strength criterion, namely when the ratio $\sigma_3 \geq \sigma_t$.

(3) Numerical model

Based on the geological conditions of the Xingelao Coal Mine, a FLAC3D model was established with dimensions of 300 m × 260 m × 107.3 m. The No. 5^{-3} coal seam working face has a strike length of 283 m and a dip length of 160 m. Both the coal seam dip angle and the working face gradient are 1°, with an average burial depth of 100.72 m. The remnant coal pillars in the No. 5^{-2} coal seam are 5 m × 5 m in width, and the width of the goaf entries (coal rooms) is 5 m. To minimize boundary effects

during model calculation, constraints were applied to restrict horizontal displacement on the front, back, left, and right sides of the model, while vertical displacement was constrained at the bottom of the model. The levels of the influencing factors are listed in Table 7. The advancing direction of the working face is set along the positive Y-axis, with a total advancement length of 160 m. As the surrounding rock cannot recover after coal seam extraction, the Mohr-Coulomb constitutive model was adopted, as illustrated in Fig. 11.

Table 7: Influencing factors level configuration table

Influencing factor	Level
Backfill strength (MPa)	2.70
Backfill ratio	0, 1/5, 1/3, 1/2, 2/3, 3/4
Face length (m)	160

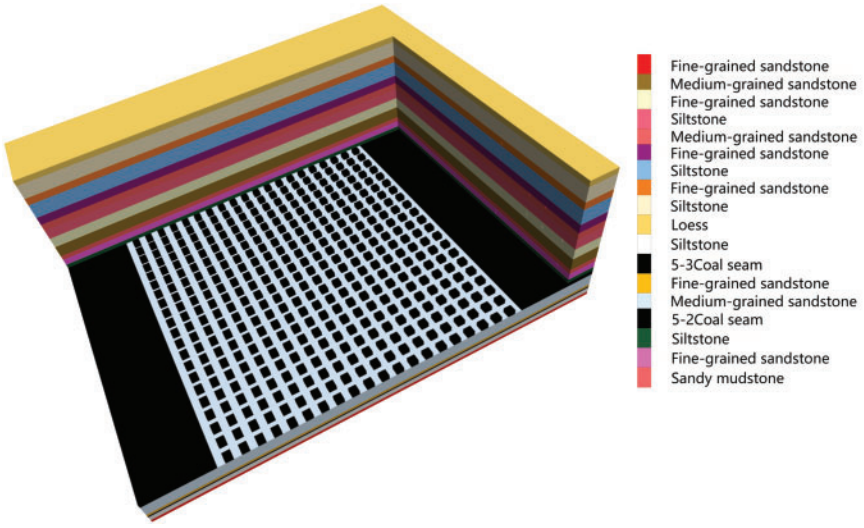

Figure 11: Numerical simulation model

(4) Experimental plan

The initial stress field of the model was first calculated. To ensure that the *in-situ* stress state of the original rock mass is accurately represented prior to excavation simulation, an initial equilibrium calculation was conducted for the model, as shown in Fig. 12.

Subsequently, room-and-pillar mining was conducted in the No. 5^{-2} coal seam, followed by stress equilibrium adjustment of the overlying strata after excavation, as illustrated in Fig. 13.

Then, the fill command was used to backfill the room-and-pillar goaf with different filling ratios, and the corresponding material parameters were assigned to the backfill (Refer to Table 8). Finally, based on this configuration, excavation of the No. 5^{-3} coal seam was carried out to investigate the stress distribution, displacement characteristics, and plastic zone failure patterns of the room-and-pillar goaf under varying backfill ratios.

Figure 12: Original rock stress cloud map

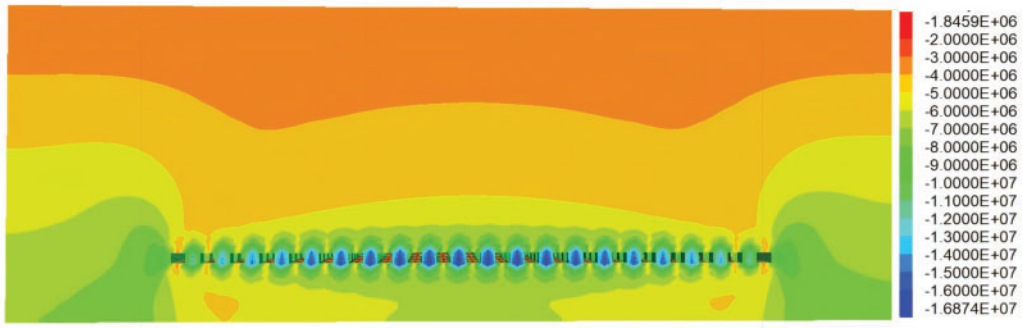

Figure 13: Stress cloud map of the house-column goaf

Table 8: Tabulated mechanical properties of backfill materials

Lithology	Uniaxial compressive strength (MPa)	Density (MPa)	Poisson's ratio	Cohesion (MPa)	Internal friction angle (°)	Proportion of backfill (Height m)
Backfill	2.70	1.02×10^3	0.30	0.23	30.0	1/5 (0.710) 1/3 (1.183) 1/2 (1.775) 2/3 (2.367) 3/4 (2.663)

4.2 Characterization of Overlying Strata Subsidence and Coal Pillar Deformation under Different Backfill Proportions

Considering the complexity of the onsite grouting filling process, it is challenging to ensure consistent changes in slurry strength, though the filling ratio can be manually controlled. Based on the findings discussed in Section 3.2 and to enhance the accuracy and reliability of the experiment while minimizing random variability, the method of controlling variables is employed. The 7 d UCS of the filling material is fixed at 2.70 MPa, while the filling ratio is varied (1/5, 1/3, 1/2, 2/3, 3/4) to examine the effect of different filling ratios on the movement of the overlying strata.

Fig. 14 illustrates the analysis of overlying strata subsidence in both the No. 5^{-3} coal seam and the No. 5^{-2} room-and-pillar goaf following the completion of mining in the No. 5^{-3} coal seam. The figure presents displacement diagrams of the overburden corresponding to various backfilling ratios: (a) 0, (b) 1/5, (c) 1/3, (d) 1/2, (e) 2/3, and (f) 3/4. Following the extraction of coal rooms in the No. 5^{-2} coal seam, part of the roof strata lost their load-bearing capacity, leading to stress redistribution on the coal pillars. Subsequent mining activities in the No. 5^{-3} coal seam caused secondary displacement of the overlying strata and induced deformation within the pillar structure. As illustrated in Fig. 14, the roof subsidence in the unfilled room-and-pillar goaf areas of the 5^{-3} and 5^{-2} coal seams reaches its maximum at the central section of the working face. This subsidence gradually diminishes towards both flanks, demonstrating a fundamentally symmetrical profile. The maximum overburden settlement was observed to be 1.15 m for the No. 5^{-3} coal seam and 1.35 m for the No. 5^{-2} coal seam. As the backfill ratio progressively increased from 0 to 3/4, the overburden subsidence in the room-and-pillar goaf exhibited significant mitigation, with the settlement decreasing sequentially to 0.87, 0.78, 0.68, 0.60, and 0.58 m. Correspondingly, these reductions reflect magnitude decreases of 35.6%, 42.2%, 49.6%, 55.6%, and 57.0%, respectively. Specifically, when the backfill ratio is below 2/3, the reduction rate of overburden subsidence is highly sensitive to incremental increases in the backfill ratio. However, once the backfill ratio exceeds 2/3, the corresponding reduction rate of subsidence shows a diminished responsiveness to further increases in the backfill ratio. The underlying reason is that when the backfill ratio reaches two-thirds, the load-bearing structural system achieves a relatively stable state. Subsequent increases in the backfill proportion yield only marginal improvements in the overall bearing capacity.

Based on the analysis of Fig. 15, when the mining step distance is less than 60 m and the backfill ratios range from 1/5 to 3/4, the movement of the overburden strata in the room-and-pillar goaf areas shows minimal impact, with subsidence magnitudes remaining essentially consistent. This phenomenon arises because the inherent strength of the No. 5^{-3} coal seam roof effectively inhibits the development of large-scale fractures before a significant roof collapse, thereby preserving relative stability in strata displacement. When the mining span exceeds 60 m, initial fractures develop in the No. 5^{-3} coal seam roof, significantly diminishing its supporting capacity for the room-and-pillar goaf. Consequently, overburden subsidence in the room-and-pillar goaf area begins to intensify. As periodic fracturing develops in the No. 5^{-3} coal seam roof, the cumulative subsidence of the overlying strata progressively increases. The subsidence magnitude of the overlying strata in the No. 5^{-2} coal seam shows significant variations under different backfill ratios. Compared to the zero-backfill scenario, the subsidence magnitudes under other backfill ratios were 64.4%, 57.8%, 50.4%, 44.4%, and 43.0%, respectively. These data clearly demonstrate that increasing backfill ratios effectively controlled strata subsidence, with the subsidence magnitude showing a progressive reduction of 35.6%, 42.2%, 49.6%, 55.6%, and 57.0% relative to the non-backfill baseline. When the backfill ratio is less than 2/3, increases in the backfill ratio lead to a significant reduction in overburden settlement. However, once the backfill ratio exceeds 2/3, further increments result in only marginal decreases in settlement. This phenomenon occurs because, at a backfill ratio of 2/3, the load-bearing structural system reaches a relatively stable state, and additional increases in the backfill ratio yield only limited improvements in overall bearing capacity.

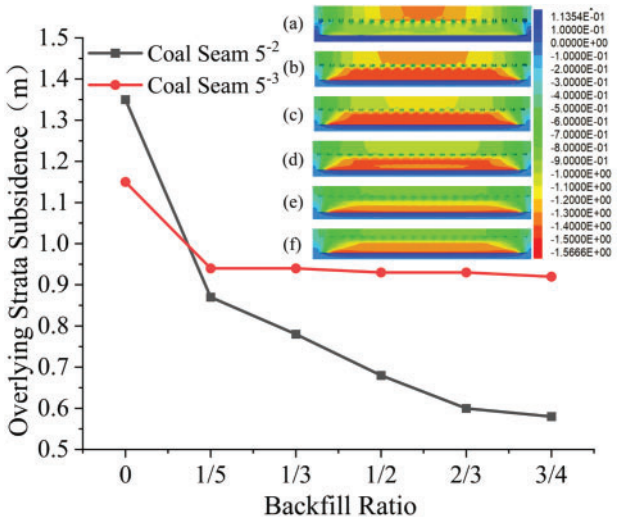

Figure 14: Diagram of overburden subsidence under different backfill ratios (a–f). (a) 0; (b) 1/5; (c) 1/3; (d) 1/2; (e) 2/3 and (f) 3/4

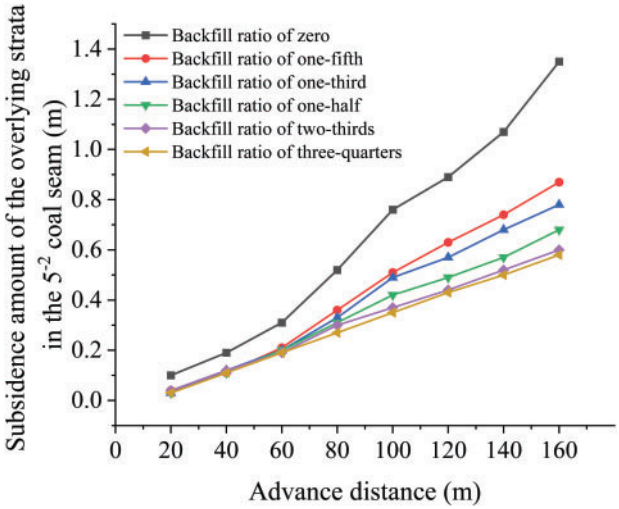

Figure 15: Diagram of overlying rock subsidence control under different backfill ratios at the same mining step

Fig. 16 illustrates the deformation characteristics of coal pillars at varying backfill ratios, while Fig. 17 presents the deformation patterns observed at different pillar positions. A comprehensive analysis of both figures indicates that significant deformation occurs after the extraction of the No. 5^{-3} coal seam. The maximum deformation is observed at the central coal pillars within the room-and-pillar goaf. The magnitude of deformation gradually decreases toward the lateral boundaries. This deformation distribution exhibits an axisymmetric configuration along the centerline of the goaf. The deformation magnitude of the central coal pillar decreased from 1.31 m under unfilled conditions to 0.89, 0.75, 0.66, 0.54, and 0.49 m following the implementation of backfill reinforcement. These values correspond to sequential reduction rates of 36.8%, 45.1%, 51.1%, 59.4%, and 61.7%, respectively. The deformation of the boundary coal pillars on both sides decreased from 0.63 m under non-backfilled

conditions to 0.48, 0.42, 0.38, 0.35, and 0.28 m following backfill reinforcement, representing reduction rates of 46.9%, 51.9%, 61.7%, 70.4%, and 72.8%, respectively. It can be concluded that backfilling treatment in room-and-pillar goaf areas effectively mitigates coal pillar deformation under repeated mining disturbances. Notably, when the backfill ratio exceeds 2/3, the reduction in pillar deformation shows a relative attenuation. This phenomenon can be attributed to a transition in the load-bearing mechanisms. When the backfill ratio is less than 2/3, the coal pillar serves as the main load-bearing component in the composite support system. It carries the majority of the overburden load. The backfill material plays a secondary role, providing auxiliary support. Under these conditions, the deformation of the coal pillar is significantly reduced. Conversely, when the backfill ratio exceeds 2/3, the backfill material assumes a larger share of the load-bearing responsibility, becoming the primary supporting component. This altered stress distribution pattern leads to a relatively smaller reduction in the deformation magnitude of the coal pillar. Therefore, the mitigation effect on coal pillars shows a pronounced diminishing trend as the backfill ratio increases further.

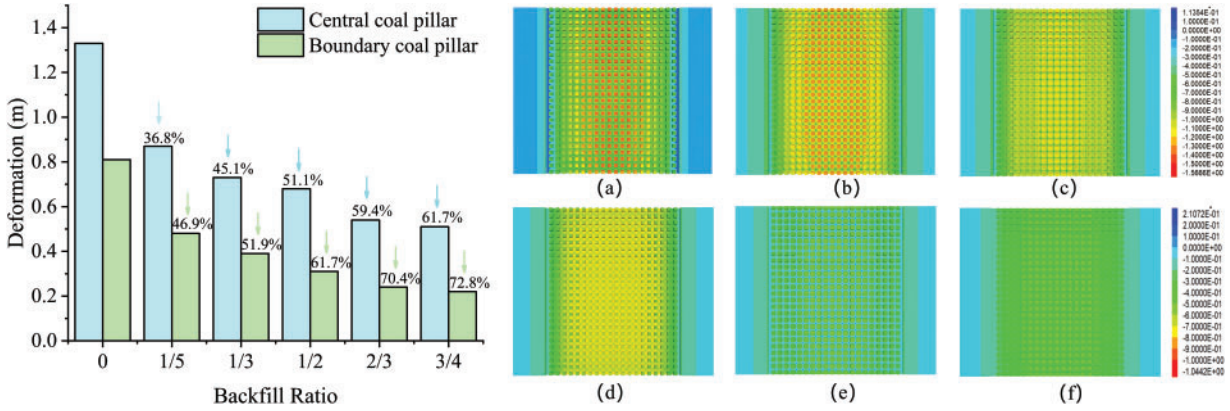

Figure 16: Deformation of coal pillars under different backfill ratios: (a) The deformation cross-sectional diagram of all coal pillars in the mined-out area when the backfilling ratio is zero; (b) The deformation cross-sectional diagram of all coal pillars in the mined-out area when the backfilling ratio is one-fifth; (c) The deformation cross-sectional diagram of all coal pillars in the mined-out area when the backfilling ratio is one-third; (d) The deformation cross-sectional diagram of all coal pillars in the mined-out area when the backfilling ratio is one-half; (e) The deformation cross-sectional diagram of all coal pillars in the mined-out area when the backfilling ratio is two-thirds; (f) The deformation cross-sectional diagram of all coal pillars in the mined-out area when the backfilling ratio is three-quarters

4.3 Stress Distribution Characteristics of Overlying Strata and Coal Pillars under Different Backfill Proportions

Quantitative analysis alone, based on the varying control effectiveness of backfill ratios on the overlying strata, is insufficient. A comprehensive assessment of the control performance of backfill ratios on the overlying strata requires the integration of stress analysis. Fig. 18 illustrates the stress contour maps of the overlying rock in the room-and-pillar goaf under various backfill ratios. As shown in the figure, after the completion of mining in the No. 5^{-3} coal seam, the stress in the overlying strata reaches a maximum in the central zone of the room-and-pillar goaf. The stress magnitude gradually decreases toward the lateral boundaries. The overburden stress at the central section decreased by 39.0%, from 11.3 MPa under non-backfill conditions to 6.89 MPa at a 3/4 backfill ratio. Similarly, the

stress at the peripheral section showed a 37.5% reduction, from 7.95 MPa without backfill to 4.97 MPa with a three-quarter backfill ratio. This backfilling configuration demonstrates a significant reduction in stress across all monitored positions within the overlying strata.

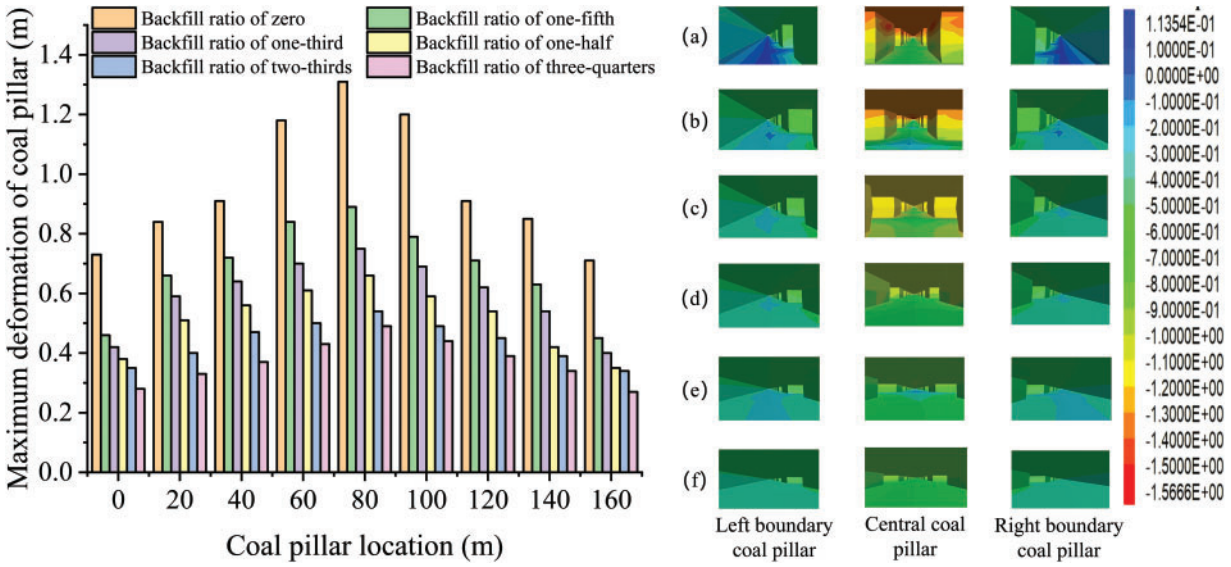

Figure 17: The deformation of coal pillars at different locations: (a) Cross-sectional view of coal pillar shape variation at different locations within the goaf when the filling ratio is zero; (b) Cross-sectional view of coal pillar shape variation at different locations within the goaf when the filling ratio is one-fifth; (c) Cross-sectional view of coal pillar shape variation at different locations within the goaf when the filling ratio is one-third; (d) Cross-sectional view of coal pillar shape variation at different locations within the goaf when the filling ratio is one-half; (e) Cross-sectional view of coal pillar shape variation at different locations within the goaf when the filling ratio is two-thirds; (f) Cross-sectional view of coal pillar shape variation at different locations within the goaf when the filling ratio is three-quarters

To further investigate the stress distribution on the coal pillar, the pillar located at the central position of the gob, where the stress is maximized, was selected for analysis. As illustrated in Fig. 19, with an increase in the filling ratio from 0 (a) to 3/4 (f), the stress concentration zone shifts from the lower-middle section to the upper-middle section. At the same time, the horizontal stress in the coal pillar decreases progressively. The maximum horizontal stress drops from 15.7 to 6.98 MPa, representing a 55.5% reduction. The minimum horizontal stress decreases from 10.2 to 5.06 MPa, corresponding to a 50.4% reduction. These findings suggest a negative correlation between the filling ratio and the stress exerted on the coal pillar.

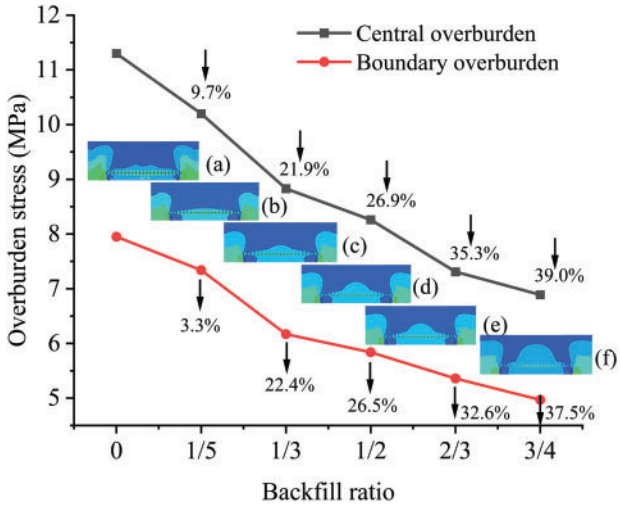

Figure 18: Stress Nephogram of overlying strata in room-and-pillar goaf under different backfilling ratios: (a) stress nephogram of overburden in the goaf when the filling ratio is zero; (b) stress nephogram of overburden in the goaf when the filling ratio is one-fifth; (c) stress nephogram of overburden in the goaf when the filling ratio is one-third; (d) stress nephogram of overburden in the goaf when the filling ratio is one-half; (e) stress nephogram of overburden in the goaf when the filling ratio is two-thirds; (f) stress nephogram of overburden in the goaf when the filling ratio is three-quarters

As shown in Fig. 20, the lower portion of the coal pillar experiences reduced vertical stress due to reinforcement by the backfill material, while the upper section becomes the primary stress concentration zone. As the backfill ratio increases, the maximum vertical stress on the coal pillar decreases from 12.14 to 5.54 MPa, representing a 54.5% reduction. These results indicate that the backfill material significantly enhances the compressive strength of the coal pillar.

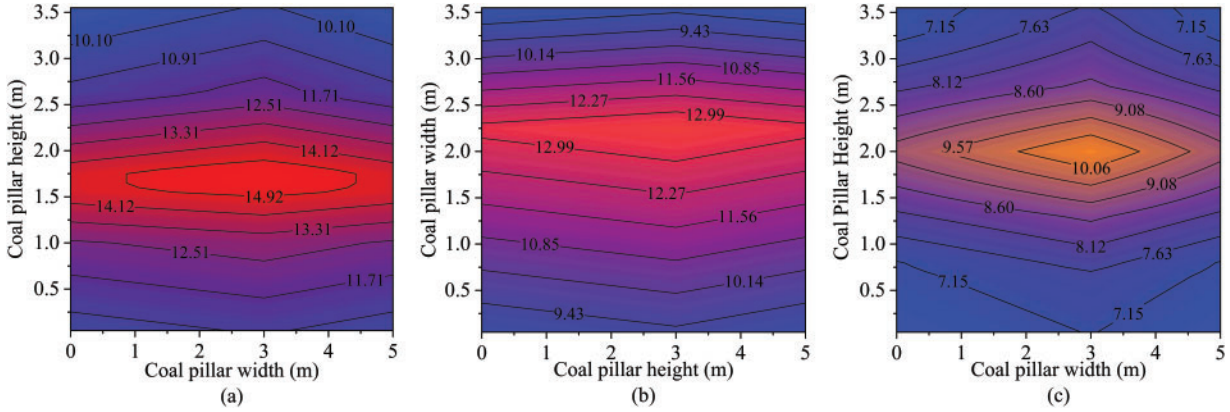

Figure 19: (Continued)

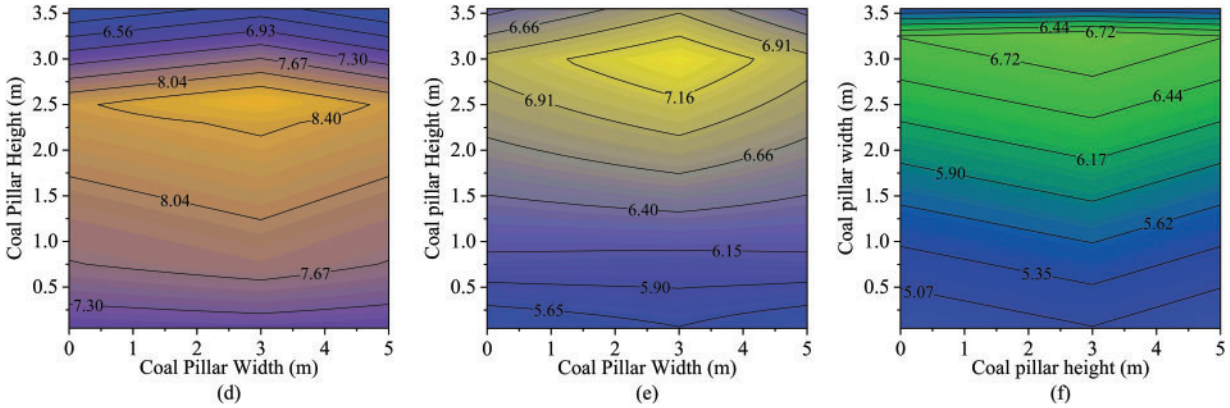

Figure 19: Horizontal stress distribution contour map of coal pillars under different backfill ratios (a–f)

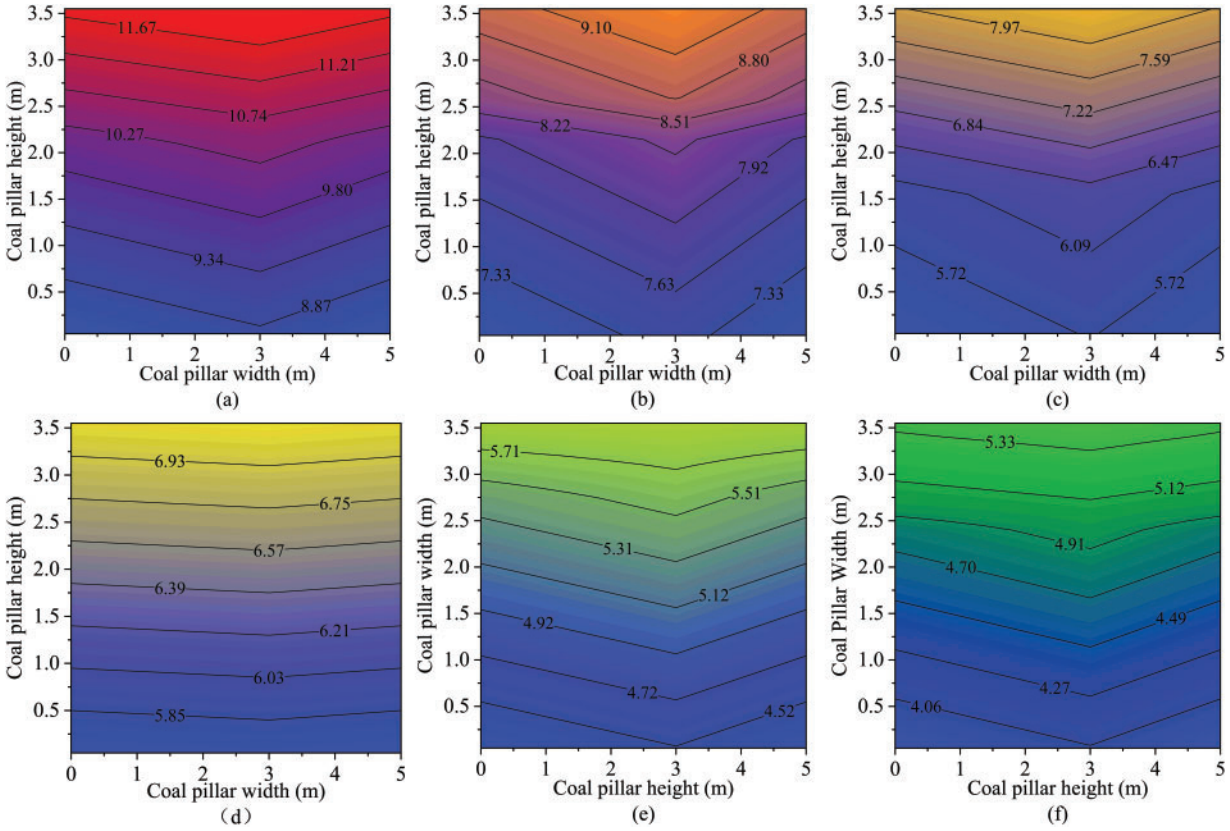

Figure 20: Vertical stress distribution contour map of coal pillars under different backfill ratios (a–f)

4.4 Failure Analysis of Coal Pillar Plastic Zone under Different Backfill Proportions

Fig. 21 illustrates the failure patterns of the plastic zones in the overlying strata and coal pillars under different backfilling ratios. As shown, at backfilling ratios of 0 (a), 1/5 (b), and 1/3 (c), the reduction in coal pillar deformation is limited. Both horizontal and vertical bearing pressures exhibit

only slight decreases. This indicates that the backfill material provides limited support after the extraction of the No. 5^{-3} coal seam. However, the plastic zones within the room-and-pillar goaf have fully penetrated the entire coal pillar structure. Complete failure is characterized by vertical damage ranging from 0 to 5 m and horizontal damage extending from 0 to 3.55 m. When the backfill ratio reaches 1/2 (d), the plastic zone of the coal pillar does not fully penetrate the entire structure. Although partial failure occurs, with damage depths ranging from 0 to 1.2 m, the pillar retains some residual bearing capacity. However, when the backfill ratio increases to 2/3 (e) and 3/4 (f), the plastic zone of the coal pillar is significantly reduced. Under these conditions, no pillar failure is observed, indicating that the backfill material effectively enhances the load-bearing capacity of the coal pillar through efficient stress transfer and confinement effects.

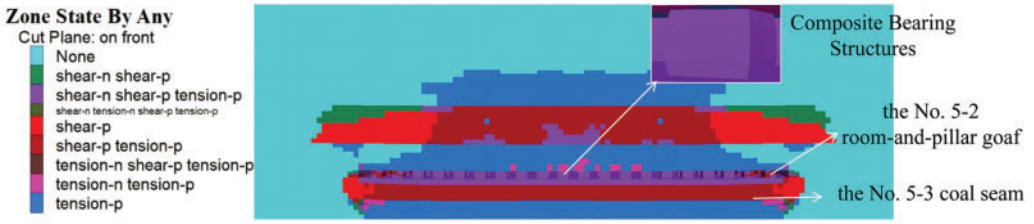

(a) backfill ratio of zero

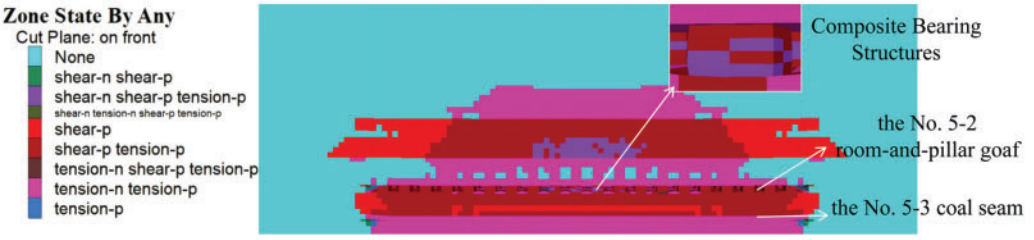

(b) backfill ratio of one-fifth

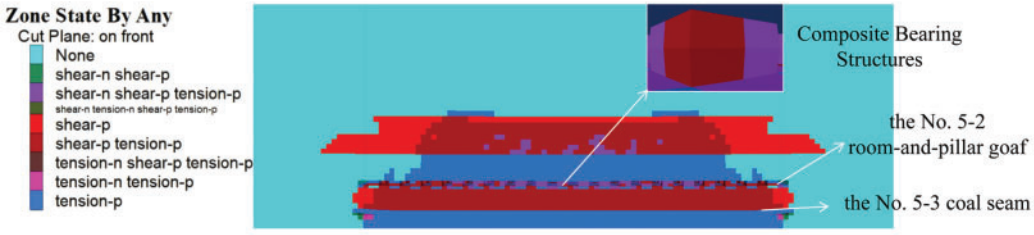

(c) backfill ratio of one-third

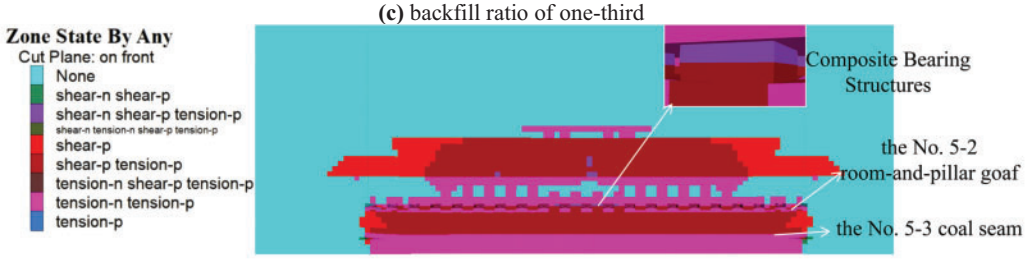

(d) backfill ratio of one-half

Figure 21: (Continued)

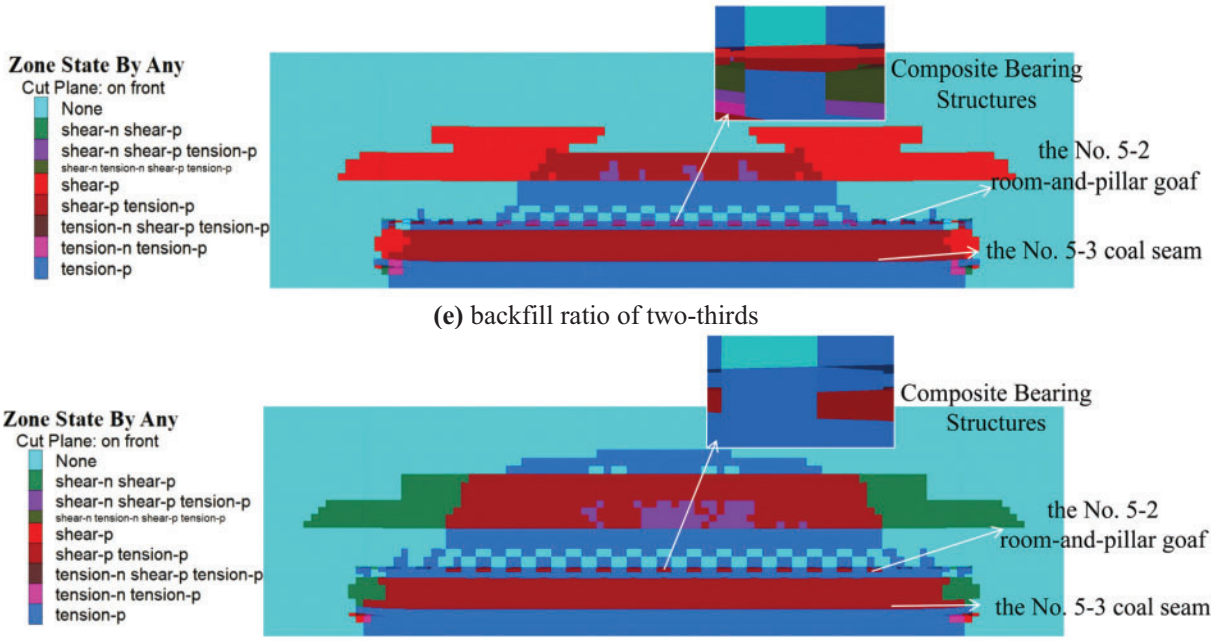

(e) backfill ratio of two-thirds

(f) backfill ratio of three-quarters

Figure 21: Failure diagrams of plastic zones in overlying strata and coal pillars under different backfilling ratios (a–f). (a) backfill ratio of zero; (b) backfill ratio of one-fifth; (c) backfill ratio of one-third; (d) backfill ratio of one-half; (e) backfill ratio of two-thirds; (f) backfill ratio of three-quarters

In conclusion, under repeated mining disturbances, grouting reinforcement in room-and-pillar goaf areas enhances the stability of coal pillars. It also contributes to effective control of overlying strata subsidence. As the backfill ratio increased from 0 to 3/4, overlying strata subsidence and coal pillar deformation decreased accordingly. Reductions were also observed in both horizontal and vertical stresses on the pillars, as well as in the extent of plastic zone development within the coal pillars. Based on the engineering conditions of the Xingelao Coal Mine, structural failure of coal pillars occurs when the backfill ratio in room-and-pillar goaf areas falls below 1/2. In this state, the pillars can no longer provide effective support for the overlying strata during the extraction of the No. 5^{-3} coal seam. This loss of support significantly increases the risk of strata subsidence and poses serious safety hazards. When the backfill ratio reaches 1/2 in room-and-pillar goaf areas, although the coal pillars do not experience complete failure and retain some partial bearing capacity, safety considerations must be prioritized in practical engineering applications. Therefore, a backfill ratio of 1/2 does not meet the required safety standards for industrial implementation. When the backfill ratio exceeds 1/2—specifically at 2/3 and 3/4—the interaction between coal pillars and backfill materials preserves the structural integrity of the pillars. This interaction also provides effective support for the overlying strata. However, practical engineering considerations related to economic viability and grouting time efficiency require a comprehensive evaluation. Based on this, it is concluded that a backfill ratio of 2/3 offers the most operationally viable compromise.

5 Conclusion

(1) A composite bearing structure model of the backfill-coal pillar system and its corresponding mechanical model were developed. Theoretical analysis was performed to evaluate the stability of the roof rock beam under two conditions: partial failure and intact coal pillar states within the composite bearing structure. The analysis indicates that when the coal pillar remains intact, the maximum roof load acting on the coal pillar occurs at the L/2 position of the goaf span, where the roof rock beam experiences its maximum bending moment, deflection, and rotation angle. In the event of coal pillar failure, the roof rock beam at point A within the goaf area simultaneously reaches its maximum bending moment, exhibiting peak deflection and angular displacement.

(2) Through orthogonal experiments on backfill strength, the optimal gradation (n = 5) for backfill materials at Xingelao Coal Mine was determined. Nine orthogonal experimental groups (S1-S9) were established, with curing results indicating compressive strengths ranging from 1.65 to 2.70 MPa at 7 days, 3.84 to 5.10 MPa at 14 days, 4.81 to 5.88 MPa at 21 days, and 5.40 to 6.88 MPa at 28 days. Through range analysis, it was determined that within the first 7 days of curing, the influencing factors on backfill performance followed the order: A > C > D > B. After the curing period exceeded 7 days, the prioritization of factors shifted to A > D > B > C. As a result, the backfill mix proportions of S7 and S8 were ultimately selected as the optimal formulations.

(3) Through mold preparation, backfill-pillar composite bearing structures were fabricated using S7 and S8 backfill mixtures at different filling ratios (1/5, 1/3, 1/2, 2/3, 3/4). Experimental results revealed that the 7-day uniaxial compressive strength of the composite bearing structures ranged from 5.81 to 7.88 MPa for S7 and from 5.99 to 8.58 MPa for S8, under varying proportion conditions. Based on theoretical verification and calculations, S8-2/3 was selected as the optimal experimental parameter, followed by a systematic analysis of the failure characteristics in the composite bearing structures.

(4) Given the engineering complexity of backfill operations and to minimize potential errors, numerical simulation software was employed to further validate the results. With a fixed backfill strength of 2.70 MPa and varying backfill ratios (0, 1/5, 1/3, 1/2, 2/3, 3/4), the maximum roof subsidence in the repeated mining-induced room-and-pillar goaf decreased from 1.35 to 0.58 m, with the reduction magnitude increasing from 35.6% to 57.0%. Simultaneously, the maximum deformation of coal pillars decreased from 1.31 to 0.49 m, exhibiting an improved reduction rate from 36.8% to 61.7%. The maximum horizontal stress in the coal pillars reduced from 15.7 to 6.98 MPa, while the maximum vertical stress decreased from 12.14 to 5.54 MPa.

(5) When the backfill ratio reaches 2/3, the load-bearing structural system achieves a relatively stable state, and further increases in the backfill proportion result in only marginal improvements in the overall bearing capacity performance. The composite bearing medium itself has an inherent elastic limit. When the backfill ratio exceeds 2/3, its compressibility exhibits minimal variation, thereby limiting its ability to effectively further mitigate subsidence of the overlying strata. The load-bearing structure undergoes a transformation based on the backfill ratio: when the filling proportion is less than 2/3, the coal pillar does not serve as the primary load-bearing component; when it exceeds 2/3, the composite load-bearing system becomes the dominant bearing entity.

Acknowledgement: The authors would like to express our sincere appreciation to the Editors and Reviewers for their valuable insights and continuous encouragement.

Funding Statement: This work was supported by the National Natural Science Foundation of China (Nos. 52174127, 52374137), the Youth Innovation Team Project of Shaanxi University, and the Outstanding Youth Science Fund Project of Shaanxi (2023-JC-JQ-42).

Author Contributions: The authors confirm contribution to the paper as follows: study conception and design: Wenyu Lv; data collection: Yongping Wu, Panshi Xie, Chao Lyu; analysis and interpretation of results: Lei Gao, Ru You, Tianqi Song; draft manuscript preparation: Lei Gao, Shijie Li. All authors reviewed the results and approved the final version of the manuscript.

Availability of Data and Materials: Data available on request from the authors.

Ethics Approval: Not applicable.

Conflicts of Interest: The authors declare no conflicts of interest to report regarding the present study.

References

1. Yao J, Han K, Zhu W, Cao YB. Research on collapse detection in old coal mine goafs based on space-sky-earth remote sensing survey. Remote Sens. 2024;16(7):1164. doi:10.3390/rs16071164.
2. Guo LJ, Tao ZG, He MC, Coli M. Impact of Micro-NPR bolt on the mining of deep-buried phosphate via the room-and-pillar method. Tunn Undergr Space Technol. 2023;140(12):105326. doi:10.1016/j.tust.2023.105326.
3. Liu H, Hao C, Wang Z, Li C, Guo L, Liang J, et al. Study on stability of underlying room and pillar old goaf in close coal seam and mining of the upper coal seam. Front Earth Sci. 2023;10:1071250. doi:10.3389/feart.2022.1071250.
4. Yang J, Chang X, Gao Y, Fu Q, Hou S, Song H, et al. Stress field comparison in deep coal mines: roof cutting versus traditional methods. Geotech Geol Eng. 2024;42(8):6809–31. doi:10.1007/s10706-024-02865-7.
5. Yang S, Guo Y, Liu Q, Guo R, Xu Y. Minimizing the damage of underground coal mining to a village through integrating room-and-pillar method with backfilling: a case study in Weibei Coalfield, China. Sustainability. 2025;17(2):602. doi:10.3390/su17020602.
6. Zhou N, Yan H, Jiang SY, Sun Q, Ouyang SY. Stability analysis of surrounding rock in paste backfill recovery of residual room pillars. Sustainability. 2019;11(2):478. doi:10.3390/su11020478.
7. Zhen Y, Bing T, Cheng HC, Gang W. Study of caving and fracturing over a longwall panel beneath a goaf mined by room and pillar. J Min Saf Eng. 2012;29(2):157–61. (In Chinese).
8. Hai KL, Ren WY, Gang LS. Analysis on overburden strata movement law of coal mining face under goaf of room and pillar mining face. Coal Sci Technol. 2015;43(5):26–9. doi:10.13199/j.cnki.cst.2015.05.007.
9. Bin SY, Wei G, Yun ZZ, Ding ZL. Research on movement pattern and support loading in fully mechanized longwall mining face beneath gob of room-pilar mining. China Coal. 2017;43(12):91–5. (In Chinese). doi:10.19880/j.cnki.ccm.2017.12.017.
10. Lee C, Chang SH, Shin HS. A study on conceptual evaluation of structural stability of room-and-pillar underground space. J Korean Tunn Undergr Space Assoc. 2013;15(6):585–97. doi:10.9711/KTAJ.2013.15.6.585.
11. Hummel M, Hummelova I, Koudelkova J, Cerna K. Mining of protection pillars without subsidence. J Min Sci. 2015;51(2):335–41. doi:10.1134/S1062739115020179.

12. Salmi EF, Nazem M, Karakus M. The effect of rock mass gradual deterioration on the mechanism of post-mining subsidence over shallow abandoned coal mines. Int J Rock Mech Min Sci. 2017;91:59–71. doi:10.1016/j.ijrmms.2016.11.012.
13. Kim J-G, Ali MAM, Yang H-S. Robust design of pillar arrangement for safe room-and-pillar mining method. Geotech Geol Eng. 2019;37(3):1931–42. doi:10.1007/s10706-018-0734-1.
14. Abbasi B. An improved rock mass behavior numerical model and its applications to longwall coal mining [master's thesis]. Carbondale, IL, USA: Southern Illinois University; 2016.
15. Baryshnikov VD, Fedyanin AS, Pul' EK, Baryshnikov DV. Geomechanical monitoring of open-pit bottom reserves in Mir Mine, ALROSA: results. J Min Sci. 2017;53(1):34–42. doi:10.1134/S106273911701180X.
16. Franqueira MF, Paneiro GA. Contribution to the geomechanical stability of marble underground openings using backfill. Earth Environ Sci. 2021;833(1):012131. doi:10.1088/1755-1315/833/1/012131.
17. O'Sullivan D. An optimization-based decomposition heuristic for solving complex underground mine scheduling problems [dissertation]. Golden, CO, USA: Colorado School of Mines; 2013.
18. Adach-Pawelus K. Influence of the roof movement control method on the stability of remnant. Earth Environ Sci. 2017;95(4):042022. doi:10.1088/1755-1315/95/4/042022.
19. Das AJ, Mandal PK, Ghosh N, Singh AP, Kumar R, Tewari S, et al. Evaluation of energy accumulation, strain burst potential and stability of rock mass during underground extraction of a highly stressed coal seam under massive strata-a field study. Eng Geol. 2023;322(9):107178. doi:10.1016/j.enggeo.2023.107178.
20. Loui JP, Sheorey PR. Estimation of non-effective width for different panel shapes in room and pillar extraction. Int J Rock Mech Min Sci. 2002;39(1):95–9. doi:10.1016/S1365-1609(01)00074-0.
21. Cheikhaoui Y, Nettour D, Cheniti H, Bensehamdi S, Chaibl R. The loading and slenderness ratio effect on the failure probability of pillars in an underground mine: case study. Procedia Struct Integr. 2023;48:81–7. doi:10.1016/j.prostr.2023.07.113.
22. Roy R, Chakraborty S, Bisai R, Pal SK, Mishra S. Gravity blind backfilling of abandoned underground mine voids using suitable mix proportion of fill materials and method of filling. Geotech Geol Eng. 2023;41(3):1801–19. doi:10.1007/s10706-022-02371-8.
23. Sharmila L, Senthil K, Raja RV. Study on the compression property of formation space for theoretical support. In: Proceedings of the 2023 Intelligent Computing and Control for Engineering and Business Systems (ICCEBS); 2023 Dec 14–15; Chennai, India. p. 1–7. doi:10.1109/ICCEBS58601.2023.10449143.
24. Kumar S, Sinha RK, Jawed M, Murmu S. Assessment of coal pillar strength under the influence of sand stowing in deep coal mines. Geotech Geol Eng. 2024;42(4):2815–31. doi:10.1007/s10706-023-02707-y.
25. Nazimko V, Zakharova L, Kusen A, Peng S. Rock pressure relief is the basic alternative for sustainable underground mining. EDP Sci. 2021;280(2):08020. doi:10.1051/e3sconf/202128008020.
26. Kostecki T, Spearing AJS. Influence of backfill on coal pillar strength and floor bearing capacity in weak floor conditions in the Illinois Basin. Int J Rock Mech Min Sci. 2015;76(1):55–67. doi:10.1016/j.ijrmms.2014.11.011.
27. Gupta AK, Paul B. A review on utilisation of coal mine overburden dump waste as underground mine filling material: a sustainable approach of mining. Int J Min Miner Eng. 2015;6(2):172–86. doi:10.1504/ijmme.2015.070380.
28. Shekhar N, Pal S, Jaiswal A, Hazara P. Numerical modelling for prediction of ground subsidence over room and pillar mining in an underground coal seam. In: Proceedings of the Indian Geotechnical Conference; 2021 Dec 16–18; Trichy, India. Singapore: Springer Nature. p. 155–65. doi:10.1007/978-981-19-6998-0_15.
29. Shanmuga PR, Sreelakshmi S, Kalyan KG. Effect of gypsum on strength behavior of lime-modified pond ash as an underground stowing material. In: Geotechnical characterisation and geoenonmentavirl engineering: IGC 2016. Vol. 1. Singapore: Springer Nature; 2019. p. 281–8. doi:10.1007/978-981-13-0899-4_35.